Revision 1: Microtexture Development During Rapid Cooling in Three Rhyolitic Lava Flows

Seaman, S.J.

Department of Geosciences, 611 North Pleasant Street, University of Massachusetts, Amherst, MA 01003, sjs@geo.umass.edu

Corresponding author:

Sheila Seaman

Department of Geosciences, University of Massachusetts, Amherst, MA 01003

e-mail: sjs@geo.umass.edu

Phone: 413 545 2822

FAX: 413 545 1200

Abstract

The effects of water concentration and degassing history on the development of spherulites and flow banding were examined in three middle Tertiary rhyolitic lava flows from the Atascosa Mountains of southern Arizona. The Hell's Gate lava flow and the Atascosa lava flow host spherulites of strongly contrasting texture, and neither are flow banded. The Sycamore Canyon lava flow is a flow banded rhyolite that hosts two populations of spherulites. Spherulites in the Hell's Gate lava flow consist of two to four generations of bladed radiating alkali feldspar crystals that increase in water concentration along their length. Needle-like radiating feldspar crystals in spherulites in the Atascosa and Sycamore Canyon lava flows are in some cases

punctuated by concentric rinds of glass that are reservoirs for water rejected by the feldspar crystals. The differences in spherulite crystal morphology between the Sycamore Canyon and Atasocosa flows (both needle-like) and the Hell's Gate flow (bladed) may reflect a more rapid cooling rate of the Sycamore Canyon and Atascosa flows. Thick gray flow bands in the Sycamore Canyon lava flow host higher water concentrations than thin orange flow bands, suggesting that flow bands are zones of greater and lesser volatile concentration, deformed by stretching of the flowing magma. Temperature was uniform across the light and dark flow bands of the Sycamore Canyon flow, indicating that water concentration, one of the variables that control diffusion coefficients, rather than temperature, controlled spherulite size in this case. Phenocrysts in the Hell's Gate lava flow are strongly resorbed, probably as a result of magma ascent along a near-adiabatic gradient that resulted in exsolution of water from the melt, and subsequent dissolution of existing quartz phenocrysts by the water-rich melt. Resumption of crystallization of anhydrous phases such as quartz and feldspar would have further enriched the melt in water, facilitating the growth of spherulites. Spherulites in two of the lava flows (Sycamore Canyon and Hell's Gate) increase in water concentration from core to rim, as would be expected in spherulites growing in melt enriched in water rejected by the growing feldspar crystals. Spherulites in the Atascosa rhyolite flow decrease slightly in water concentration from core to rim, possibly because the magma degassed during spherulite growth. Calculation of water concentration profiles in spherulites from all three rhyolite flows on the basis of Rayleigh fractionation of water between sanidine and rhyolitic melt shows that the very high water concentrations in spherulites (typically >0.6 * water concentration in surrounding glass) cannot be accounted for by Rayleigh fractionation. Instead it is likely that sanidine incorporated water as fluid inclusions and/or as 'water clusters'during rapid crystal growth. Water concentration profiles in the glass surrounding spherulites do not preserve the high concentration zone at the spherulite boundary that has been observed in younger lava flows, so that spherulite growth rates cannot be calculated on the basis of mass balance calculations of distribution of water during spherulite growth. Rather, the water concentration profile in the surrounding glass is a half plateau, the height of which is approximately equivalent to the far field water concentration in the surrounding glass, indicating that water that accumulated at the spherulite/magma boundary diffused sufficiently rapidly to equilibrate with the surrounding magma as the lava flow cooled.

Introduction

Lava flows are the most abundant volcanic features on the surfaces of the terrestrial planets. In our solar system, rhyolitic lava flows may be peculiar to Earth. Compared to basaltic flows that cover the ocean floors, they are volumetrically smaller, but they cover vast tracts of young felsic volcanic terranes, and they are present throughout the geologic record. They are spatially and temporally associated with ignimbrite deposits that resulted from more spectacular explosive eruptions. However, in contrast to relatively monotonous thick ignimbrites, rhyolitic lava flows host an abundance of complex textural features that provide information about the degassing, ascent, and emplacement history of the flow, with implications for entire volcanic provinces.

Flow banding and spherulites are two prominent and visually striking textural features of lava flows. Both features preserve information about the ascent, degassing, and eruption history of the magma (e.g., Seaman et al., 1995; Tuffen et al., 2003; Gonnermann and Manga, 2003; Castro et al., 2005a and b; Castro et al., 2007; Castro et al., 2008; Watkins et al., 2009). One approach to interpreting the information preserved in these features is investigation of compositional variations in and around features such as flow bands and spherulites. The accumulation of water at the interface between growing spherulites and surrounding melt has received considerable attention in recent literature (Castro et al., 2008; Watkins et al., 2009; Seaman et al., 2009), and a recent contribution (Castro et al., 2009) shows that hydrogen generated by magnetite crystallization in spherulites reduces the iron in rinds of glass surrounding spherulites. The work summarized here focuses on possible interdependence of spherulite growth, the development of flow banding, and the concentration of water in rhyolitic lava flows. Three rhyolitic lava flows from the middle Tertiary Atascosa Mountains of southern Arizona are nearly identical in composition, but are texturally distinct. One of these lava flows hosts both flow banding and spherulites, and the other two host only spherulites of strongly contrasting texture. We show that water concentration variations, both locally and within the entire rhyolitic flow, were an essential factor in the development of these contrasting textural features.

Methods

Samples

Three lava flows from the middle Tertiary Atascosa Mountains of southern Arizona (Figure 1) were examined in this study. The three deposits are located in the same volcanic succession within the complex, and all erupted between ~23 and 26 Ma (Seaman and McIntosh, 1999). They were chosen for this study because of their strongly contrasting textures (Figure 2) and nearly identical major and trace element compositions (Table 1). One of these, the Sycamore Canyon flow, was described in a separate study (Seaman et al., 2009). Table 2 provides a general comparison of textural features of the three flows.

The Hell's Gate rhyolite flow The Hell's Gate rhyolite flow does not host flow bands. Rather, it consists of rust red spherulites ranging from 1.2-3.0 mm diameter, in a matrix of unwelded white perlitic glass. The spherulites are texturally complex, consisting of delicate radiating sheaths of skeletal crystals that form successive growth layers, each nucleated on the preceding layer (Figure 3a). The centers of spherlites may be a crystal or a crystal fragment or may consist of only radiating feldspar crystals. Radiating crystals are long and bladed, with ends that come to a point (Figure 3b). The widest bladed crystals (approximately 10 microns) are in the generation closest to the center of the spherulite. Successive generations of crystals become progressively thinner (to about 2 microns in width). Up to four generations of radiating crystals have been identified in single spherulites. The edges of radiating feldspar crystals are defined by feathery entrainments of magnetite crystals (Figure 3b). These entrainments of oxide grains become more complexly branched farther from the core of the spherulite. Layers of glass between zones of radiating feldspar crystals are entirely absent in the Hell's Gate rhyolite flow.

Phenocrysts in the Hell's Gate rhyolite flow are quartz and alkali feldspar. They are approximately 0.5 to 3.0 mm in diameter. In most instances they have rounded edges and/or deep embayments (Figure 3c). Quartz phenocrysts are more abundant than sanidine phenocrysts (approximately 5% compared to <1% of the rock) and they are considerably larger than sanidine phenocrysts. Quartz phenocrysts are subrounded and deeply fractured, giving them a soccer ball-like appearance (Figure 3d). Sanidine phenocrysts are typically euhedral and near-rectangular. Quartz phenocrysts commonly host melt inclusions that look much like the surrounding spherulite material (Figure 3e).

Spherulites and phenocrysts make up approximately 60% of the volume of the Hell's Gate rhyolite flow. The remainder consists of crumbly perlitic glass (Figure 3d). The perlitic glass zones consist of devitrified subrounded regions bordered by the curved, glass-filled fractures that are characteristic of perlites. Phenocrysts in the perlite zones are cut by the curved fractures that give the perlite its distinctive appearance.

The Sycamore Canyon rhyolite flow The Sycamore Canyon rhyolite flow hosts flow bands that are typically up to 0.5 m long. They terminate at zones of offset between flow bands, and they vary in sinuosity from quite planar throughout most of the flow to very convoluted in discrete zones. The Sycamore Canyon lava flow consists of alternating flow bands of two distinct colors (Figure 4a). Light-colored, gray flow bands (henceforth referred to as 'light flow bands') are thicker (3-5 mm) than darker, orange bands (henceforth referred to as 'dark flow bands') that are 1 to 2 mm thick (Figure 4a). Light flow bands consist of large spherulites (400-600 microns in diameter) surrounded by gray glass and sparse fine quartz and sanidine crystals. Spherulites in the light flow bands consist of radiating feldspar crystals and fine-grained magnetite (Fig. 4b). The core of the light spherulites consists of a void, a sanidine crystal, or a granular mixture of quartz and feldspar. Most spherulites in the light flow bands show a single growth layer of radiating feldspar/quartz growth. A few percent of the large spherulites show an inner radiating feldspar/quartz zone that is separated from one or two concentric outer feldspar/quartz zones by one or two concentric rings of gray glass.

Dark flow bands consist of orange glass, much smaller spherulites (~200 microns in diameter) and sparse sanidine and quartz crystals. Spherulites in the dark flow bands typically consist of a glassy core, with acicular feldspar and quartz crystals radiating outward (Figure. 4c),

(DOI will not work until issue is live.) DOI: http://dx.doi.org/10.2138/am.2013.4313

but in some cases a crystal occupies the center of the spherulite, and feldspar crystals radiate out from the crystal. The radiating zone ends in an abrupt, well-defined edge, and a layer of orange glass typically concentrically coats the spherulite (Figure 4c). Glassy gray-brown border regions discontinuously separate the flow bands (Fig. 4a) and in some instances, also host sparse small (20-30 μm in diameter) spherulites. Unlike many flow-banded rocks that have been described by other workers (e.g., Smith 2002; Castro et al. 2005a), flow bands in the Sycamore Canyon lava flow are not defined by differences in microlite concentrations. Rather, the difference in color between the orange and the gray flow bands appears to be a true difference in the color of the glass phase in the flow bands, and it may indicate a difference in oxidation state of iron, as described by Castro et al. (2009) for oxidation state differences in glass rinds surrounding spherulites. However, again, in contrast to the Aliso lava flow (Seaman et al., 1995) and the Katrurajima, Japan flow (Smith, 2002), the flow bands in the Sycamore Canyon lava flow are not interpreted to be bands of mingled magma.

Phenocrysts in the Sycamore Canyon flow are sparse and small (to 0.1 to 0.5 mm diameter). As in the other flows, they consist of quartz and sanidine. In contrast to phenocrysts in the Hell's Gate flow, those in the Sycamore Canyon flow are generally euhedral.

The Atascosa rhyolite flow Like the Hell's Gate rhyolite flow, the Atascosa rhyolite flow does not host flow bands. The size of the spherulites (400 microns to 1 cm diameter) in the Atascosa lava flow ranges more widely than those of either of the other flow banded lavas. Unlike the Sycamore Canyon flow, which has two size populations of spherulites, the spherulites of the Atascosa rhyolite flow are distributed between the small and large end-members. In contrast to the Hell's Gate rhyolite flow, the Atascosa rhyolite flow has a strongly welded, non-perlitic matrix that hosts spherulites that are concentrically zoned in terms of both color and texture (Figure 5a). Intense welding may be a result of the high temperature of the lava flow, or of post-eruptive interaction with silica-saturated hydrothermal fluid. The low phenocryst abundance in the Atascosa lava flow is consistent with a high initial temperature of the Atascosa flow. The skeletal crystals that make up the spherulites are not delicate feldspar sheaths like those of the Hell's Gate rhyolite flow. Rather, they are needle-like crystals similar to those in the spherulites of the Sycamore Canyon rhyolite flow (Figure 5b). In contrast to the spherulites of the Sycamore Canyon rhyolite flow, the majority of those in the Atascosa rhyolite flow are concentrically zoned in terms of color, with from two to four alternating white and salmon-colored shells (Figure 5a). In some cases, a concentric layer of glass separates radiating concentric layers of crystals (Figure 5c), and in other cases, the crystal zones are not separated by glass zones (Figure 5a). In some instances, a single generation of radiating skeletal crystals begins on a glass layer and extends over more than one color zone. Spherulites in the Atascosa flow have a very distinct outermost rind and a larger, typically granular-textured core. The largest spherulites in the Atascosa flow are larger (~ 1 cm diameter) than those in either of the other lava flows. Both radial and mudcrack-patterned fractures are common in the Atascosa flow.

Phenocrysts in the Atascosa rhyolite flow, like those of the other two rhyolite flows, are quartz and alkali feldspar. Phenocrysts are considerably less abundant in the Atascosa rhyolite flow than in the Hell's Gate flow, and are smaller (~0.25-1.0 mm) in the Atascosa rhyolite flow. As in the Hell's Gate flow, both sanidine and quartz are present, but quartz is considerably more abundant. In contrast to the Hell's Gate flow, the majority of phenocrysts do not host prominent

This is a preprint, the final version is subject to change, of the American Mineralogist (MSA)
Cite as Authors (Year) Title. American Mineralogist, in press.
(DOI will not work until issue is live.) DOI: http://dx.doi.org/10.2138/am.2013.4313

melt inclusions, and those that are present are not as fresh in appearance as those in the Hell's Gate flow.

Analytical Methods

Identification of water in glass and in spherulites is based on FTIR spectroscopy. Spectra were collected in the Infrared Spectroscopy Laboratory in the Department of Geosciences at the University of Massachusetts, using infrared radiation generated by a globar source. A Bruker Vertex 70 spectrometer was used with a Hyperion 3000 microscope. The system has both a single element detector for collection of single spectra, and a 64 x 64 focal plane array detector for mapping chosen areas of samples. The array of detectors permits rapid and high-resolution collection of images of concentrations of water species. In this study, spectra were collected in the mid-IR range (1000-4000 cm^{-1}) using a KBr beamsplitter. The spectrometer is purged with nitrogen gas, and nitrogen gas flows onto the sample stage, in order to reduce the contribution of atmospheric water and carbon dioxide to analyses.

The samples are self-supported thin slices of rock of conventional thin section dimensions, and 0.120-0.183 mm thick. The rock slices are optically transparent so that one can easily be certain that the infrared beam is passing through only a single crystal during an analysis. Standard thin sections were prepared, except that acetone-soluble epoxy (Crystalbond) was used for cementing the rock to the glass slide. After polishing to the appropriate thickness, each slide was placed in an acetone bath until the rock slab separated from the glass. Each slab was carefully extracted from its acetone bath and allowed to dry thoroughly before analysis. Exact (+/- 1 μm) thickness of samples was determined by measurement with a Starrett #733 digital micrometer. The slabs were placed between two glass slides into which a 1 cm-diameter central hole had been drilled. FTIR spectra were first examined to ensure that they did not include bands indicative of C-H groups, which would indicate the presence of undissolved epoxy that might contain exotic water. Spectra were collected on discrete points in spherulites, in glass, and in feldspar crystals. Spot sizes ranged from 8 x 8 μm to 20 x 20 μm, depending on the size of the target. Spectra were typically collected using 64 scans, and a polynomial flexicurve baseline correction was applied prior to calculation of peak heights and areas.

The imaging process involves the collection of data across the entire spectral range, in 64 x 64-pixel blocks. Each pixel represents approximately a 2.6 x 2.6-micron square of the sample. After collection of the image, the user chooses a spectral region of interest, and the map then displays concentration variations only in that spectral range. Concentration maps included in this work show total water concentration as represented by the broad OH^- stretching band that extends from approximately 2900 to 3700 cm^{-1}.

Total water concentration is related to the area under the peak representing the band of interest, the thickness of the sample, and the molar absorption coefficient by the Beer-Lambert Law:

$$A = c * t * \varepsilon, \qquad (1)$$

where *A* is the total band area measured from spectra from each of the three mutually perpendicular sections, *c* is the concentration of the species, *t* is the thickness, and *ε* is the molar absorption coefficient. The following form of the Beer-Lambert Law was used for calculating water concentration in glass (Stolper, 1982):

$$c = (18.02 * \text{Absorbance}) / (t * D * \varepsilon) \qquad (2)$$

This is a preprint, the final version is subject to change, of the American Mineralogist (MSA)
Cite as Authors (Year) Title. American Mineralogist, in press.
(DOI will not work until issue is live.) DOI: http://dx.doi.org/10.2138/am.2013.4313

where *c* is the weight fraction of water, *18.02* is the molecular weight of water, *absorbance* is the height of the absorption peak, *t* is thickness in cm, and *D* is density in g/liter, and *ε* is absorption coefficient, in liters/mol-cm . The 3535 cm^{-1} (2.8 μm) band, which represents fundamental OH^- stretching, was used by Stolper (1982) and many subsequent workers (e.g. Dixon et al. 1988; Dixon and Clague 2001; Saito et al. 2001) to determine total water concentration. In this study, we have used the height of this band, which commonly extends from approximately 2900 cm^{-1} to 3700 cm^{-1}, to calculate water concentration in glass (Stolper, 1982; Dixon et al., 1988; Ohlhorst et al., 2001; Mandeville et al., 2002). Several workers (e.g., Stolper, 1982; Newman et al., 1986; Zhang et al., 1997; Ohlhorst et al., 2001; Mandeville et al., 2002) have established molar absorption coefficients for both near-IR (5200 cm^{-1} and 4500 cm^{-1}) bands and mid-IR (3200-3500 cm^{-1}) bands in a wide range of glass compositions. In this study, absorption coefficients for the glasses differ for each lava flow, and are based on the Si + Al mole fraction of the glass (Mandeville et al., 2002; King et al., 2004).

The following form of the Beer-Lambert Law was used to calculate water concentration in crystals (Libowitzky and Rossman, 1997):

$$c = A * 1.8 / (t * D * \varepsilon) \qquad (3)$$

where *c* is concentration in wt% H_2O, *A* is area under the absorption peak in cm^{-1}, *1.8* is a factor used to express hydrogen concentrations as their equivalent water concentrations, *t* is thickness in cm, *D* is density g/cm^3, and ε is the absorption coefficient in cm^{-2}/mole H_2O L^{-1}.

The absorbance used in this study to calculate water concentration in crystals is the integrated area under the peak(s) that occur between 3700 and 3100 cm^{-1}, following Libowitzky and Rossman (1997) and Johnson and Rossman (2003). Both the feldspar phenocrysts and the radiating skeletal crystals in spherulites in the lava flows are sanidine feldspar, so the absorption coefficient used for calculating water concentration in the crystals is that derived by Johnson and Rossman (2003) for calculating water concentration in feldspar crystals. They established a value of 107000 +/- 5000 L mol^{-1}-cm^{-2} as a universal feldspar absorption coefficient, and demonstrated its application to sanidine feldspars (Johnson and Rossman, 2003 and 2004).

For anisotropic phases (such as feldspar), quantitative determination of water concentration requires collection of FTIR spectra from measurement in three mutually orthogonal orientations and summing of concentrations measured in each orientation (Libowitzky and Rossman 1997; Johnson and Rossman 2003). The concentrations are related to the sum of the area under the peaks at each of the three orientations using the value of ε for a given mineral group. Even the excellent resolution provided by the Bruker instrument is not sufficient to allow for the collection of spectra from individual skeletal crystals that make up the spherulites in the Sycamore Canyon and Atascosa flows, so collection of spectra from individual skeletal crystals in three mutually perpendicular orientations was not possible for this study. Water concentrations calculated from area under the total water peak using the Beer Lambert law were multiplied by three to approximate total sanidine water concentration. Because sanidine is a moderately anisotropic mineral, the true water concentration varies in each of the three principal directions, so concentrations derived from simple multiplication of water concentration derived from measurement in one orientation are an approximation. Radiating sanidine crystals in spherulites of the Hell's Gate flow are wide enough to permit analysis of single crystals. For these spherulites, spectra were collected in two mutually perpendicular orientations within the plane of the thin sections, but total water concentration was calculated by using the average of the concentrations calculated from the two orientations to estimate the concentration in the third orientation. The concentrations associated with each of the three orientations were then summed to provide total water concentration.

Precision of analyses of total water in glass is approximately +/- 5%. Dixon et al. (1991) and Dixon and Clague (2001) estimated the accuracy of total water analyses at +/- 10% based on the accuracy of absorption coefficients.

Results

Imaging of water concentration variations

Hell's Gate Rhyolite Flow The most striking result shown by imaging of water concentration in spherulites in the Hell's Gate rhyolite flow is the variation in water concentration from the cores to the rims of spherulites. There are generally three to four generations of successively thinner blade-like feldspar crystals from the core to the rim of the spherulites. Within single bladed crystals, water concentration varies, generally increasing, from the interior of the spherulite, toward the rim. There are some oscillations in water concentration. Overall, however, from the core to the rim, across all of the generations of crystals present, the water concentration increases (Figures 6 and 7). Finally, water concentration increases appear to occur in many cases abruptly rather than gradually, even when they occur within the length of a single generation of crystals rather than at the boundary where one generation ends and another begins. However, the most abrupt changes in water concentration do indeed occur at the boundaries between generations of crystals.

Sycamore Canyon Rhyolite Flow The relationships between variations in water concentrations and flow bands and spherulites in the Sycamore Canyon rhyolite flow have been described in detail in another contribution focused entirely on that subject (Seaman et al., 2009). Water concentration in spherulites is not uniform, but generally increases from cores to rims (Figure 6). Thicker gray flow bands that host large spherulites have more abundant water than the thinner orange flow bands that host small spherulites (Figure 8).

Atascosa Rhyolite Flow Spherulites in the Atascosa rhyolite flow typically have a diffuse white center region that consists of a mixture of feldspar and glass. Water concentration is nearly uniform or increases from the center outward across these zones (Figure 6). Bladed feldspar crystals form the next zone. In contrast to the bladed feldspar crystals of the Hell's Gate lava flow, water concentration generally decreases along the length of these crystals, although oscillations in water concentration also occur along crystal lengths. A few ramps of glass typically radiate out from the glass rind and across the bladed feldspar zone. These glass ramps generally have water concentrations similar to that of the interior glass rind from which they radiate, and hence are less hydrous than the bladed crystals that they intersect. The outermost zone is a second or third generation of bladed feldspar, with lower water concentration than that of any of the interior zones. The final bladed feldspar zone is separated from the inner bladed feldspar zone by a very thin, discontinuous glass rind that is more hydrous than either of the feldspar zones that it separates (Figure 6).

Quantitative analyses of water concentration variations

Hell's Gate Rhyolite Flow Single point analyses of features in the Hell's Gate rhyolite flow show that water concentrations in spherulites range from approximately 2500 ppm in the core crystals to approximately 3500 ppm in a region near the outermost boundary (Table 3). Melt inclusions in phenocrysts generally contain 2500-3000 ppm water, although one outlier contains approximately 9000 ppm water. The glass that surrounds has water concentration ranging from 3300-6500 ppm.

Sycamore Canyon Rhyolite Flow Water distribution is quite heterogeneous in the Sycamore Canyon rhyolite flow, and the details are presented in another paper (Seaman et al., 2009). However, four domains can be considered in terms of the water concentration and distribution (Table 3). First, large spherulites in light bands, have an average of approximately 2885 ppm water; small spherulites in dark bands have an average of 739 ppm water; light glass surrounding large spherulites in light bands averages 5185 ppm, and, finally, dark glass surrounding small spherulites in dark bands averages 3620 ppm water.

Atascosa Rhyolite Flow Single point analyses of features in the Atascosa rhyolite flow show that water concentrations in spherulites is slightly higher in the interior of the spherulites, and decreases to the rim, but that water concentration variation is not large (~1000 ppm) across the spherulites, ranging from ~1000-3000 ppm (Table 3). Water concentrations are near 1500-2500 ppm in interior glass zones in most spherulites, and bladed sanidine crystals host ~2500-3000 ppm near the interior glass to 1000-1500 ppm near the edge of the spherulites. Concentric glass rinds within spherulites have water concentrations up to 8000 ppm. Interstitial quartz crystals host 160-2000 ppm water. Water concentration in glass surrounding spherulites ranges from 4500 to 6500 ppm.

Spherulite Crystallization Kinetics and Cooling Rates

The three lava flows described here contrast in two ways with those for which cooling rates were modeled by Watkins et al. (2009) and Castro et al. (2008) using an advection-diffusion model: 1) spherulites in all three of the lava flows studied here host large concentrations of water; those in both the Watkins et al. (2009) and the Castro et al. (2008) studies were modeled on the basis of anhydrous spherulites and 2) water concentrations in the glass adjacent to the spherulites in the three lava flows in this study generally describe a half-plateau, the height of which is the water concentration in the far field glass, rather than the high water concentration ridge described in the Watkins et al. (2009) and Castro et al. (2008) studies at the spherulite/glass boundary.

An advection-diffusion model cannot be applied to the three lava flows studied here because 1) the spherulites are water-rich, so the condition that the water that originally occupied the space later occupied by the spherulite has been displaced to the outside of the spherulite is not valid, and, more importantly, 2) the far-field water concentration in the surrounding glass cannot be distinguished from the spherulite-adjacent water concentrations (i.e., diffusive equilibration of water throughout the surrounding glass has occurred). Despite our inability to calculate the rate of spherulite growth, the distribution of water in and around the spherulites in the three lava flows provides some information about the development of spherulites and flow banding.

Water-Rich Spherulites

The first questions raised by the observations of water-rich spherulites and diffusive equilibration of water between the near-spherulite and the far field setting are: why do the spherulites contain large concentrations of water, and can any information be taken from their water concentrations? The ratio of *average* water concentration in the spherulites to that in the surrounding glass, with the exception of the dark bands in the Sycamore Canyon rhyolite, is 0.56-0.70. Because spherulites in both the Sycamore Canyon and Atascosa rhyolites host glass as well as sanidine crystals, the water concentration in the Hells Gate spherulites, which are entirely composed of sanidine crystals, best represents water hosted by spherulite crystals only. The ratio of water in spherulite to water in surrounding glass for the Hells Gate rhyolite is approximately 0.68. Obviously this ratio cannot represent a partition coefficient for water between sanidine and rhyolitic melt. A sanidine/rhyolitic melt partition coefficient for water has not been determined, but Johnson (2005) determined a plagioclase feldspar/andesitic melt partition coefficient for water of 0.004, several orders of magnitude smaller than the proportionality preserved in these concentration profiles. Nor does it seem likely that a significant amount of water diffused *from* the surrounding glass *into* sanidine crystals in the spherulites, either as structural water or as fluid inclusions since crystallization of the sanidine. Rather, the abundance of water in the sanidine crystals in the spherulites provides information about the spherulite-forming process.

Calculation of the amount of water that would be housed in spherulites as they grow to occupy their final volume if water were entirely partitioned into the sanidine crystal structure as a trace compound, in each of the three rhyolitic lavas, was done following Philpotts and Ague (2009). If the fraction of sanidine (that makes up the spherulites) formed at a given time is F, and if the fraction of remaining melt is (1-F), and the total amount of water in the melt is c_{water}^{melt} (1-F), and if dF is the incremental amount by which the spherulites grow, then the amount of water that partitions into the sanidine, and is lost from the melt with each incremental amount of spherulite growth is:

$$-d\,[(c^{san}_{water} / K^{san/melt})(1-F)]/dF \qquad (4)$$

Rearranging,

$$-K^{san/melt}_{water} = (dc^{san}_{water} / dF) - c^{san}_{water} - F\,(d\,c^{san}_{water}/dF) \quad (5)$$

Integrating both sides of equation 5 yields:

$$\ln c^{san}_{water} / (1-K) = -\ln (1-F) + \text{constant} \quad (6)$$

When F = 0, $c^{san}_{water} = c^{o\ melt}_{water} K^{san/melt}$, where $c^{o\ melt}$ is the initial concentratin of water in the melt before the spherulites began to grow. Therefore the constant of integration is:

$$\ln (c^{o\ melt}_{water} K^{san/melt}) / (1-K) \quad (7)$$

Then $\ln c^{san}_{water} = -\ln (1-F) = \{[\ln (c^{o\ melt}_{water} K^{san/melt})]/(1-K)\} \cdot (1-K)$ (8)

The results of these calculations for each of the three rhyolitic lava flows, including both the dark and light flowbands in the Sycamore Canyon lava flow, are shown in Figure 9. It is obvious that most of the large concentrations of water in the spherulites are not the result of water partitioning into the sanidine crystal structure from the rhyolitic melt.

The most plausible explanation for the large ratio of water in spherulite crystals to surrounding glass is that much of the water in the sanidine crystals may be either in fluid inclusions, or may be water "clusters", < 1 micron in size (Johnson, 2006), as opposed to structural water that replaces K^+ or occupies a defect in the crystal lattice (Johnson, 2006). Alkali feldspar crystals have been documented to host up to approximately 1000 ppm of structural H_2O and OH^-, and more than 1000 ppm as fluid inclusions (Johnson, 2006). Submicroscopic fluid inclusions are shown by a broad, isotropic peak at ~3440 cm^{-1}, and water in sanidine is marked by a broad, isotropic peak at ~3400 cm^{-1} (Johnson and Rossman, 2004). Water in spherulite crystals is almost certainly a mixture of structural water and fluid inclusion water, both representing primary magmatic water. It must be emphasized that the water in the sanidine crystals was incorporated during spherulite growth; no mechanism in known that could have introduced secondary fluid inclusions into non-fractured, pristine bladed sanidine crystals in the Hell's Gate lava flow.

Water in sanidine produces FTIR spectra with broad bands centered at 3400 cm^{-1} and 3250 cm^{-1} with maximum absorption parallel to X, and at 3060 cm^{-1} with maximum absorption parallel to Y (Johnson and Rossman, 2003). Water in fluid inclusions produces a broad isotropic band centered at 3440 cm^{-1} with a shoulder at 3270 $cm^{-}1$ (Johnson and Rossman, 2004). In this study, the broad, "total water" FTIR band for spherulites from the Hells Gate flow is centered at approximately 3250 cm^{-1} and that for rhyolitic glass is broad and asymmetric and centered at approximately 3050 cm^{-1}. For the Sycamore Canyon rhyolite, spherulites from both thin dark light flowbands and thick light flowbands, the FTIR peak is broad and centered at approximately 3450 cm^{-1}, and that of the surrounding glass is centered at approximately 3250 cm^{-1}. Spherulites in the Atascosa rhyolite have a broad water peak with plateau centered at ~3250-3450 cm^{-1}; that of the glass is centered at approximately 3250 cm^{-1}. Hence, it is in most cases difficult to distinguish water in fluid inclusions from structural water (either replacing K^+ or housed in defects) in sanidine in spherulites. The distinction between structural and fluid inclusion water (or water clusters) is not critical to this study. In either case, the water became part of the sanidine crystals in the spherulites as they grew rapidly in the water-hosting rhyolitic melt. Fluid inclusions, representing water that exsolved at low pressure from the rhyolitic melt, were captured by the crystals as they grew, and some water molecules partitioned into the sanidine structure, becoming part of the sanidine crystal lattice.

The maximum concentration of water that could be represented by fluid inclusions in sanidine crystals has been calculated based on the height of the pertinent FTIR bands as summarized above. A molar absorption coefficient of 115+/- 6 L/mol-cm, from Clunie et al.

(1966), for water in fluid inclusions, used by Johnson and Rossman (2004) in their survey of water in feldspar, was used in the Beer Lambert equation to calculate water concentrations in sanidine crystals. If all of the water occurred as fluid inclusions, this calculation indicates that the amount of water is 0.60 to 0.68 of the amount calculated on the assumption that all of the water is structural water. The range of proportion of fluid inclusion to structural water exists because structural water in feldspar crystals is calculated on the basis of area under the total water peak, while water concentration in fluid inclusions is calculated on the basis of height of the total water peak. The shape of the peak varies slightly, causing the proportionality in water concentration to vary from one sample point to another. Use of the molar absorption coefficient of Thompson (1965), which is 81 L/mol-cm, rather than that of Clunie et al. (1966) in the Beer-Lambert Law produces values for fluid inclusion water that are approximately equal to the values calculated on the assumption that all water is structural water (3348 ppm water as fluid inclusion water compared to 3507 ppm water as structural water, for example).

Diffusion of Water From the Spherulite/Glass Boundary

In this case, the spherulites grew rapidly enough that sanidine crystals incorporated as fluid inclusions water that had exsolved from the magma, along with water that was partitioned into sanidine crystals as structural water or OH^-. Concentration profiles across spherulites and surrounding glass for all three rhyolite flows (Figure 6) shows that despite the incorporation of water in sanidine crystals and glass in spherulites, water accumulated at the spherulite/glass boundary, as shown by other workers (Castro et al. (2008) and Watkins et al. (2009). However, the contrast in water concentration between spherulite and surrounding glass is much smaller in the three lava flows described here than in the lava flows examined in the other two studies for two reasons. First, as discussed above, in all three of the lava flows studied here, significant water was retained in the spherulites as structural water and fluid inclusion water. The spherulites in the studies of Castro et al. (2008) and Watkins et al. (2009) are modeled on the basis of anhydrous spherulites, although Castro et al. (2008) pointed out that in one of their samples spherulites retained water, and attributed it to water in glass and in microvesicles. Second, the half-plateau shape of the water concentration profiles in the glass adjacent to the spherulites in the present study indicates that water that was probably abundant at the conclusion of spherulite formation in the glass at the spherulite/glass boundary has diffused away from that boundary over the past 25 million years, such that the concentration of water at the boundary is very similar to the far field water concentration in the surrounding glass. Diffusion rates were calculated at a range of temperatures to determine whether the water concentration at the spherulite/glass boundary could have equilibrated with the far-field water concentration as the lava flow cooled. The diffusion distance is proportional to the square root of time (Zhang, 2010):

$$x \sim= (Dt)^{0.5} \qquad (9)$$

where D is the diffusion coefficient in m^2/sec and t is time in seconds. Water occurs in non-reduced melts as OH^- and as H_2O. At total water concentrations less than ~0.2 wt.% water, most water occurs as OH^-. Diffusion coefficients were calculated for each lava flow (Table 3) at temperatures bracketing the probable glass transition temperature (620-750°C; Swanson et al., 1989; Manley, 1992; Westrich et al., 1988; Castro et al., 2008), using the equation for metaluminous rhyolitic melts with <1 wt.% water at 773°K and <3 wt.% water at 1473°K from Ni and Zhang (2008):

$$D_{H2O}^{total} = C_w \exp(-18.10 + 1.888P - ((9699 + 3626P)/T)) \qquad (10)$$

where C_w is water concentration in weight percent (calculated for each lava flow on the basis of mass balance between average water concentrations of spherulites and glass), P is pressure in GPa (0.0001 GPa was used in all calculations) and T is temperature in ^oK. Diffusion distances from the spherulite/glass interface differ between rhyolite flows, and within the flow banded Sycamore Canyon flow, because diffusion coefficients are dependent on water concentrations (Table 4). Using the Hell's Gate flow as an example, diffusion distances range from 519 microns per day at 850^{o}C to 160 microns per day at 700^{o}C (the approximate glass transition temperature). Gottsmann and Dingwell (2001) calculated the cooling rate of the frontal flow ramp of the Roche Rosse rhyolitic flow in Lipari, Italy. They determined cooling rates of 0.2 to 0.03^{o}K per minute in this part of the flow, but pointed out that cooling rates of less than tens of degrees per day would be necessary to sustain flow in a highly viscous rhyolitic magma. Using a conservative scenario of the Hell's Gate lava flow cooling at a rate of 10^{o}K per day, and extruding at 1123^{o}K, 15 days would be required to reach an approximate glass transition temperature of 923^{o}K. Over this time period, the distance traversed by the diffusion front would range from 519 microns per day to 160 microns per day. Even at the slow end of this range, water would travel more than two mm from the spherulite/glass boundary, a distance greater than the distance between spherulites. As a result, the ambient water concentration of the glass is preserved at the spherulite/glass boundary.

Spherulite Growth Laws

Both Castro et al. (2008) and Watkins et al. (2009) calculated growth rates of spherulites based on the balance between the growth rate of spherulites and diffusion of water in the surrounding magma. Both chose diffusion-controlled spherulite growth laws because growth of spherulites is limited by the diffusion rates to the growing spherulite of ions necessary for spherulite growth, and possibly by the diffusion rates away from the spherulite boundary of ions rejected by the spherulite. Castro et al. (2008) observed that larger spherulites grew faster than smaller spherulites. Castro et al. attributed this to size-dependent growth rates. Watkins et al., citing two spherulites of differing size, suggested that a higher average D for the larger spherulite would account for it growing larger across the same time interval as the smaller spherulite. D is dependent on temperature, so Watkins et al. suggested that contrasting spherulite sizes reflect contrasting temperature histories rather than size-controlled growth rates.

The Sycamore Canyon lava flow hosts two size populations of spherulites. Large spherulites are confined to lighter colored flow bands, and small spherulites are confined to darker colored flow bands. The entire rock consists of tightly spaced light and dark flow bands, suggesting that it is unlikely that neighboring flow bands cooled under contrasting temperature conditions, leading to contrasting diffusion coefficients (D). Diffusion coefficients are also dependent on the water concentration in the melt (equation 11). Both the spherulites and the flow bands in the Sycamore Canyon lava flow host contrasting water concentrations. Water concentrations in both spherulites and glass in the dark bands are lower than in the spherulites and glass in the light bands. These relations strongly suggest that, at least in the Sycamore Canyon lava flow, spherulite growth is ultimately water concentration-controlled rather than size- or temperature-controlled

Flow banded and non-flow banded rhyolite flows

Seaman et al. (2009) suggested that flow bands represent more and less water-rich zones of a felsic magma that underwent extension during flow, and that, if water concentration in the melt had been greater, water in the water-richer zones would perhaps have exsolved to produce vesicles. Both Castro et al. (2008) and Watkins et al. (2009) cited instances of spherulites both overgrowing and deflecting flow bands. In the Sycamore Canyon lava flow, flow banding developed before spherulites formed, on the basis of the confinement of small orange spherulites to thin orange flow bands, and of large gray spherulites to thick gray flow bands. It is possible that flow banding facilitates the escape of water from the melt, resulting in a relatively dry melt. The Tumacacori rhyolitic lava flow, in the same volcanic complex from which the three samples examined here were collected, is a flow-banded rhyolite in which flow bands commonly have lens-shaped interior vesicles in which thundereggs grew in apparently formerly gas-filled voids. These textures suggest that flow bands can be collapsed planar vesicles. Collapse of the vesicles occurs before the growth of the spherulites that are then confined to that flow band. Flow banding may indicate situations in which water concentration in rhyolitic magmas was heterogeneously distributed, and almost sufficient for vesiculation to occur at near-surface pressure.

Crystal Morphology in Spherulites

Spherulite appearance and water concentration relations are quite different in each of the three rhyolite flows. The Sycamore Canyon and Atascosa rhyolite flows both host spherulites composed of skeletal, needle-like crystals. Crystals in the Hell's Gate rhyolite flow are artistically arranged, bladed, tapering sanidine crystals that overgrow one another in a concentric arrangement. Feathery magnetite entrainments are a major feature in the Hell's Gate flow; larger magnetite crystals occur in the other flows but they occur as scattered crystals.

We attribute the contrasting morphology of feldspar crystals (needle-like vs bladed) to cooling rate, and hence growth rate of the crystals. Lofgren (1971) demonstrated that needle-like crystal morphology indicates growth in response to extremely rapid cooling rate, while bladed crystals represent growth in response to a lesser degree of undercooling. These observations suggest that the Sycamore Canyon and Atascosa lava flows cooled more rapidly than the Hell's Gate flow. The increase in crystal aspect ratio (i.e. evolution from bladed to more needle-like) from the interior to the exterior of spherulites in the Hell's Gate flow suggests that cooling rate increased over the growth interval of the spherulites. The termination of crystals at some distance from the center of the spherulite, and nucleation of a new, thinner generation of crystals, suggests that growing crystals reach a threshold cooling rate at which crystal width must be adjusted, resulting in growth of the next generation of crystals.

Water concentration increased both gradually along the length of sanidine crystals from the interior to the exterior of spherulites, and abruptly at boundaries between generations of crystals, indicating that water concentration build-up may have been a factor in defining boundaries between generations of sanidine crystal growth in spherulites.

Phenocryst Morphology

Phenocrysts in both the Sycamore Canyon and the Atascosa rhyolite flows are generally euhedral to subhedral. In constrast, those in the Hell's Gate rhyolite flow are rounded and strongly embayed, suggesting that they underwent that resorption occurred prior to spherulite growth. Resorption of quartz and feldspar can occur as a result of either semi-adiabatic magma ascent or as a result of invasion of the quartz and/or feldspar-bearing magma chamber by hotter magma (Johannes and Holtz, 1996; Müller et al., 2009). No evidence, such as mafic enclaves or xenocrysts appropriate to less evolved magmas, has been identified in the Hells Gate lava flow, so semi-adiabatic magma ascent is examined here. Three possible ascent paths of a quartzbearing rhyolitic magma with 2 wt.% water are illustrated in Figure 10 (after Johannes and Holtz, 1996 and Müller et al., 2009) and were described by Johannes and Holtz (1996) and Müller et al. (2009), as summarized here. At 800 MPa the magma consists of 50% crystals and 50% melt. Path A is the 'typical' cooling and crystallization path of a melt, along which the temperature drops and minerals encounter their solidus as the magma rises and the ratio of crystals to melt increases. Along Path B, the magma ascends with a constant ratio of crystals to melt, although the proportion of quartz to feldspar changes. By the time the solidus is reached, the proportion of quartz in the melt has decreased from 13.5 wt.% to 7.5 wt.% (Johannes and Holtz, 1996 and Müller et al., 2009). Path C is an adiabatic path along which water is released from the melt in a closed system. Higher water activity in the melt causes resorption of crystals and formation of additional melt. For path C, approximately 30 volume % of quartz and feldspar would dissolve between 800 and 50 MPa (Johannes and Holtz, 1996 and Müller et al., 2009). At the same time, quartz and feldspar would crystallize, rejecting water and causing vesiculation that hastens magma ascent. The magma would reach the granite solidus at sufficiently shallow depth that extrusion would be likely. Decompression melting is ultimately a consequence of exsolution of water from the melt, which lowers the melting temperature of crystals in the melt.

Quartz and feldspar resorption textures in the Hell's Gate lava flow suggest that the magma ascended to the surface on a path similar to Path B or C described above. An increase in water concentration in the melt caused by crystallization of quartz and feldspar may have facilitated the nucleation and growth of spherulites after resorption of early formed quartz phenocrysts.

Conclusions

Water concentration profiles across spherulites and surrounding glass in the three middle Tertiary lava flows from the Atascosa Mountains of southern Arizona confirm the observations of earlier workers (Castro et al., 2008; Watkins et al., 2009; Seaman et al., 2009) that water that is rejected by growing spherulites accumulates at the spherulite/glass boundary. In contrast to younger rhyolites studied by Castro et al. (2008) and Watkins et al. (2009), spherulites in these three lava flows 1) host significant water, and 2) do not retain a rind of high water concentration in the glass adjacent to the spherulite; rather, water concentration profile adjacent to spherulites is a half plateau, the height of which is approximately that of the far field water concentration in the surrounding glass. Water was incorporated into the rapidly growing spherulites is in the form of primary fluid inclusions and structural water. Comparison of the rate of water diffusion with cooling rates of rhyolitic lava indicate that over the cooling interval from a reasonable extrusion temperature (850^{o}C) to an approximate glass transition temperature (~700^{o}C), a water front that accumulated at a spherulite/magma boundary would travel more than two mm from that boundary, a distance greater than the distance between spherulites. As a result, the ambient water concentration of the far field glass is preserved at the spherulite/glass boundary.

Two types of flow bands in the Sycamore Canyon flow host two contrasting sizes of spherulites, and both spherulites and glass in the small spherulite-bearing flow bands host less water than those in the large spheruite-bearing flow bands. Castro et al. (2008) showed that larger spherulites grow faster than smaller spherulites, and attributed this to size-dependent growth rates. Watkins et al. (2009), attributed differences in spherulite size to higher average D for larger spherulites, which they suggested to result from higher temperatures producing larger diffusion coefficients. Temperature was uniform across the thin flow bands of the Sycamore

Canyon flow, indicating that water concentration, the other variable that controls diffusion coefficients, rather than temperature, controlled spherulite size in this case.

Flow bands of contrasting water concentrations may represent more and less water-rich zones of a felsic magma that underwent extension during flow. If water concentration in the melt had been greater, water in the water-richer zones would perhaps have exsolved to produce vesicles. Flow banding in the Sycamore Canyon lava flow developed before spherulites formed. Flow banding may indicate situations in which water concentration in rhyolitic magmas was heterogeneously distributed, and almost sufficient for vesiculation to occur at near-surface pressure.

Differences in spherulite crystal morphology between the Sycamore Canyon and Atasocosa flows (both needle-like) and the Hell's Gate flow (bladed) reflect the more rapid cooling rate of the Sycamore Canyon and Atascosa flows. The evolution from bladed to more needle-like crystals from the interior to the exterior of spherulites in the Hell's Gate flow suggests that cooling rate increased over the growth interval of the spherulites. Periodic nucleation of new, thinner generations of crystals in the Hell's Gate spherulites suggests that growing crystals reach a threshold cooling rate at which crystal width must be adjusted, resulting in growth of the next generation of crystals. Water concentration increased both gradually along the length of sanidine crystals from the interior to the exterior of spherulites, and abruptly at boundaries between generations of crystals, indicating that water concentration build-up may have been a factor in defining boundaries between generations of sanidine crystal growth in spherulites.

Water concentration is generally zoned from the interior to the rim of spherulites in all three lava flows. In the Sycamore Canyon and Hell's Gate flows, water concentration increases outwards, as would be expected in a situation where water is being rejected by anhydrous spherulite minerals as they grow. The mildly reversed zoning in water concentration in spherulites in the Atascosa flow may indicate that a late-stage degassing event was occurring at least locally as the spherulites grew, or that the spherulites grew so rapidly that water was not rejected by the crystals, but rather incorporated both as structural water and fluid inclusions.

Resorbed quartz and feldspar phenocrysts in the Hell's Gate lava flow may have resulted from ascent of the magma along a near-adiabatic path along which water exsolved from the melt and caused resorption of phenocrysts. Further increase in water concentration in the melt resulting from crystallization of additional quartz and feldspar may have facilitated the growth of spherulites.

Comparison of the three contemporaneous lava flows shows that slight variations in initial water concentration, timing of degassing, rate of cooling, and late-stage water concentration exert fundamental controls on rhyolite microtextures.

Acknowledgements

The manuscript was greatly improved by suggestions from two anonymous reviewers, from associate editor Bjorn Mysen, and from Michael Williams. This work was both begun and completed during GAIN Writing Retreats supported by NSF grant EAR 0620101, for which the author is enormously grateful.

Figure Captions

Figure 1. Map showing location of the three rhyolite flows examined in this study in the middle Tertiary Atascosa-Tumacacori volcanic complex, southern Arizona. HG: Hell's Gate lava flow; SC: Sycamore Canyon lava flow; A: Atascosa lava flow.

Figure 2.A Photograph of Hell's Gate lava flow.

B. Photograph of Sycamore Canyon lava flow.

C. Photograph of Atascosa lava flow

Figure 3. A. Spherulites in the Hell's Gate rhyolite flow consist of successive concentric layers of bladed feldspar crystals with wispy entrainments of magnetite crystals.

B. Spherulite that appears to have nucleated on a central quartz crystal

C. Spherulite without an obvious central object upon which nucleation occurred

D. Quartz crystals hosted by perlitic glass

E. Quartz phenocrysts in the Hell's Gate rhyolite flow typically are rounded and deeply embayed and host melt inclusions very similar to matrix glass in terms of both appearance and water concentration.

Figure 4. A. Flow bands in the Sycamore Canyon rhyolite flow are defined by differences in color and in spherulite size.

This is a preprint, the final version is subject to change, of the American Mineralogist (MSA)
Cite as Authors (Year) Title. American Mineralogist, in press.
(DOI will not work until issue is live.) DOI: http://dx.doi.org/10.2138/am.2013.4313 8/29

B. Large spherulite in a light band. Spherulites that grew in light bands show one to three generations of skeletal feldspar crystals. Glass rinds separate growth layers of skeletal crystals in spherulites that have more than one growth zone of crystals.

C. Small spherulite in a dark band. Spherulites that grew in dark bands have only one layer of skeletal feldspar crystals, surrounded by a glassy outer rind.

Figure 5. A. Concentrically zoned spherulite from the Atascosa rhyolite flow. The layers are defined by color changes. In some cases, generations of skeletal crystals begin and end where color changes occur; in other cases, skeletal crystals extend across more than one color zone.

B. Needle-like feldspar crystals in a spherulite

C. Spherulite from the Atascosa rhyolite flow in which glass rinds occur between generations of skeletal feldspar crystals.

Figure 6. Water concentration maps of spherulites, with water concentration profiles and X-ray maps of K, Na, and Si concentration. All plots are based on water concentration values in Table 3, which provides number of data points represented by each plot. Water concentration in spherulites is calculated for water occurring as structural water in sanidine crystals; if it were calculated as fluid inclusion water, concentrations would range from 60% to 100% of the concentrations shown, depending on molar absorption coefficient chosen for fluid inclusion water (see discussion in text). Heavy black line indicates location of traverse. On water concentration maps, blue indicates lowest water concentration and red indicates highest concentration.

A. Hell's Gate lava flow. Note general increase in water concentration from core to rim of spherulites and half plateau of water concentration at the spherulite/glass boundary. Sanidinedominated spherulites are more potassic, more sodic, and less calcic than surrounding glass. Spherulites have more sodic interiors and less sodic rims. K is enriched in spherulite rinds relative to spherulite interiors.

B. Sycamore Canyon lava flow. Note that water concentration is higher in both the spherulites and the glass of the light flow bands compared to the dark flow bands. Water concentration variation across spherulites corresponds to zones of sanidine crystals (lower water concentration) and rinds of glass (higher water concentration).

C. Atascosa lava flow. Note that water concentration in the spherulites decreases overall from the core of the spherulite to the rim. This indicates degassing of the magma as the spherulites crystallized. Sawtooth pattern of water concentration in the spherulite reflects zones of sanidine crystals (lower water concentration) and rinds of glass (higher water concentration).

All plots are based on water concentration values in Table 3, which provides number of data points represented by each plot.

Figure 7. Photograph of a spherulite from the Hell's Gate lava flow, with location of water concentration maps A and B shown. Blue indicates lowest water concentration and red indicates highest concentration. Note: 1) the overall increase in water concentration from the interior to the rind of the spherulite; 2) abrupt changes in water concentration, both along the length of crystals and at boundaries between generations of crystals, and 3) minor oscillations in water concentration from the core to the rind of the spherulite.

Figure 8. Photomicrograph of flow bands in the Sycamore Canyon rhyolite flow and map of water concentration across the thick (light) and thin (dark) flow band over the same area, showing higher water concentration (warmer colors) in thicker flow bands.

Figure 9. Plot of water concentration partitioned into sanidine crystals in spherulites calculated using a distribution coefficient for water between sanidine and melt of 0.004. Red = Atascosa lava flow, teal = Sycamore Canyon lava flow: light bands, blue = Hell's Gate lava flow, green = Sycamore Canyon lava flow: dark bands. The calculated water concentration in sanidine crystals is much lower than the measured water concentration in the crystals, supporting the suggestion that much of the water in the crystals is in primary fluid inclusions that were incorporated into the crystals as they grew rapidly during quenching of the rhyolitic magma.

Figure 10. Magma ascent paths of rhyolitic melt with 2 wt.% water, after Johannes and Holtz (1996) and Müller et al. (2009). Complete explanation of diagram is provided in text. Resorption of quartz and feldspar phenocrysts in the Hell's Gate lava flow suggests that the magma followed a path similar to B or C, during which water exsolved from the magma on the way to the surface and caused partial dissolution of phenocrysts.

References

Castro, J.M., Dingwell, D.B., Nichols, A.R.L., and Gardner, J.E. (2005a) New insights on the origin of flow bands in obsidian. In: M. Manga and G. Ventura (Editors), Kinematics and Dynamicas of Lava Flows. Special Paper 396. Geological Society of America, Boulder, CO, pp. 55-65.

Castro, J.M., Manga, M., and Martin, M.C. (2005b) Vesiculation rates of obsidian domes inferred from H_2O concentration profiles. Geophysical Research Letters, 32, L21307, doi:10.1029/2005GLO24029.

Castro, J.M., Beck, P., Cottrell, E., and Tuffen, H. (2007) Spherulites record crystallization, degassing, and oxidation-reduction mechanisms in obsidian flows. Eos Trans. American Geophysical Union, 88 (52) Fall Meeting Supplement, Abstract V14A-07.

Castro, J.M., Beck, P., Tuffen, H., Nichols, A.R., Dingwell, D.B., and Martin, M.C. (2008) Timescales of spherulite crystallization in obsidian inferred from water concentration profiles. American Mineralogist, 93, 1816-1822.

Castro, J.M., Cottrell, E., Tuffen, H., Logan, A.V., and Kelley, K.A. (2009) Spherulite crystallization induces Fe-redox redistribution in silicic melt. Chemical Geology, 268, 272–280.

Clunie, J.S., Goodman, J.F., and Ogden, C.P. (1966) Extinction coefficient of water at 2.93 μ and water content of black foam films. Nature, 209,1192-1193.

Dixon, J.E.and Clague, D.A. (2001) Volatiles in basaltic glasses from Loihi seamount, Hawaii: evidence for a relatively dry plume component. Journal of Petrology, 42, 627-654.

Dixon, J.E., Stolper, E., and Delaney, J. (1988) Infrared spectroscopic measurements of CO_2 and H_2O in Juan de Fuca Ridge basaltic glasses. Earth and Planetary Science Letters, 90, 87-104.

Dixon, J.E., Clague, D.A., and Stolper, E.M. (1991) Degassing history of water, sulfur, and carbon in submarine lavas from Kilauea volcano, Hawaii. Journal of Geology, 99, 371-394.

Gibson, R.G. and Naney, M.T. (1992) Textural development of mixed, finely porphyritic silicic volcanic rocks, Inyo Domes, eastern California. Journal of Geophysical Research, 97, 4541-4559.

Gonnermann, H.M.and Manga, M. (2003) Explosive volcanism may not be an inevitable consequence of magma fragmentation. Nature, 426, 432-435.

Gottsmann, J. and Dingwell, D.B. (2001) The cooling of frontal flow ramps: a calorimetric study of the Rocche Rosse rhyolite flow, Lipari, Aeolian Islands, Italy. Terra Nova, 13, 157-164.

Granasy, L., Pusztai, T., Gyorgy, T., Warren, J., and Douglas, J. (2005) Growth and form of spherulites. Physical Review E, 72, 011605.

Johannes, W. and Holtz, F. (1996) *Petrogenesis and Experimental Petrology of Granitic Rocks*. Springer, Berlin, Heidelberg, New York.

Johnson, E.A. and Rossman, G.R. (2003) The concentration and speciation of hydrogen in feldspars using FTIR and ^{1}H MAS NMR spectroscopy. American Mineralogist, 88, 901-911.

Johnson, E.A., and Rossman, G.R., (2004) A survey of hydrous species and concentrations in igneous feldspars. American Mineralogist, 89, 586-600.

(DOI will not work until issue is live.) DOI: http://dx.doi.org/10.2138/am.2013.4313

Johnson, E.A. (2005) Magmatic water contents recorded by hydroxyl concentrations in plagioclase phenocrysts from Mount St. Helens, 1980-1981. Geochimica et Cosmochimica Acta, 69), A743.

Johnson, E.A. (2006) Water in nominally anhydrous crustal minerals: speciation, concentration, and geologic significance. In H. Keppler and J.R. Smith (Eds.) Water in Nominally Anhydrous Minerals. Reviews in Mineralogy and Geochemistry, 62, 117-154

Kesler, S.E. and Weiblen, P.W. (1968) Distribution of elements in a spherulitic andesite. American Mineralogist, 53, 2025-2035

King, P. L., McMillan, P. F. and Moore, G. (2004) Infrared spectroscopy of silicate glasses with application to natural systems. *In*: King, P. L., Ramsey, M. S. and Swayze, G. A. (eds.) Infrared Spectroscopy in Geochemistry, Exploration Geochemistry and Remote Sensing. Mineralogical Association of Canada, Short Course 33, 93-133.

Libowitzsky, E. and Rossman, G.R. (1997) An IR absorption calibration for water in minerals. American Mineralogist, 82, 1111-1115

Lofgren, G.E. (1971) Spherulitic textures in glassy and crystalline rocks. Journal of Geophysical Research, 76, 5635-5648.

Mandeville, C.W., Webster, J.D., Rutherford, M.J., Taylor, B.E., Timbal, A., and Faure, K. (2002) Determination of molar absorptivities for infrared absorption bands of H_2O in andesitic glasses, American Mineralogist, 87, 813-821.

Manley, C.R. (1992) Extended cooling and viscous flow of large, hot rhyolite lavas: Implications of numerical modeling results. Journal of Volcanology and Geothermal Research, 53, 27–46.

Müller, A., van den Kerkhof, A. M., Behr, H.-J., Kronz, A., Koch-Müller, M. (2009): The evolution of late-Hercynian granites and rhyolites documented by quartz - a review. - Earth and Environmental Science Transactions of the Royal Society of Edinburgh, 100, Special issue 1-2, 185-204

Newman, S., Stolper, E.M,, and Epstein, S.(1986) Measurement of water in rhyolitic glasses: calibration of an infrared spectroscopic technique. American Mineralogist, 71, 1527-1541

Ni, H. and Zhang, Y. (2008) H2O diffusion models in rhyolitic melt with new high pressure data. Chemical Geology, 250, 68-78.

Ohlhorst, S., Behrens, H., and Holtz, F. (2001) Compositional dependence of molar absorptivities of near-infrared OH^- and H_2O bands in rhyolitic to basaltic glasses. Chemical Geology, 174, 5-20.

Philpotts, A.R.and Ague, J. (2009). Principles of Igneous and Metamorphic Petrology (second edition). Prentice Hall, Englewood Cliffs, New Jersey, 667p.

Saito, G., Kazahaya, K., Shinohara, H., Stimac, J., and Kawanabe, Y. (2001) Variation of volatile concentration in a magma system of Satsuma-Iwojima volcano deduced from melt inclusion analyses. Journal of Volcanology and Geothermal Research, 108, 11-31.

Seaman, S.J. and McIntosh, W.C. (1999) Mid-Tertiary silicic volcanism in south-central Arizona; the Atascosa-Tumacacori-Cerro Colorado complex. Abstracts with Programs, Geological Society of America 31, 262.

Seaman, S.J., Scherer, E.E., and Standish, J.J. (1995) Multi-stage magma mixing and mingling and the origin of flow banding in the Aliso Lava Dome, Tumacacori Mountains, southern Arizona. Journal of Geophysical Research, 100, 8381-8398.

Seaman, S.J., Dyar, M.D., and Marinkovic, N, (2009) The effects of heterogeneity in magma water concentration on the development of flow banding and spherulites in rhyolitic lava Journal of Volcanology and Geothermal Research, 183, 157-169

Smith, J.V. (2002) Structural analysis of flow-related textures in lavas. Earth-Science Reviews, 57, 279-297.

Stolper, E. (1982) Water in silicate glasses: an infrared spectroscopic study, Contributions to Mineralogy and Petrology, 81, 1-17.

Swanson, S.E., Naney, M.T., Westrich, H.R., and Eichelberger, J.C. (1989) Crystallization history of Obsidian Dome, Inyo Domes, California. Bulletin of Volcanology, 51, 161–176.

Thompson, W.K. (1965) Infrared spectroscopic studies of aqueous systems Part I. Molar extinction coefficients of water, deuterium oxide, deuterium hydrogen oxide, aqueous sodium chloride and carbon disulphide. Transactions of the Faraday Society, 61,2635-2640.

Tuffen, H., Dingwell, D.B., and Pinkerton, H. (2003) Repeated fracture and healing of silicic magma generate flow banding and earthquakes? Geology, 31, 1089-1092.

Tuttle, O.F. and England, J.L. (1955) Preliminary report on the system SiO_2-H_2O. Bulletin of the Geological Society of America, 66, 149-152.

Watkins, J., Manga, M., Huber, C., and Martin, M.C. (2009) Diffusion-controlled spherulite growth in obsidian inferred from H_2O concentration profiles. Contributions to Mineralogy and Petrology, 157, 163-172.

Westrich, H.R., Stockman, H.W., and Eichelberger, J.C. (1988) Degassing of rhyolitic magma during ascent and emplacement. Journal of Geophysical Research, 93, 6503–6511.

Zhang, Y. (2010) Diffusion in minerals and melts: theoretical background. In Y. Zhang and D. J. Cherniak (Eds.) Diffusion in Minerals and Melts. Reviews in Mineralogy and Geochemistry 72, 5-59.

Zhang, Y., Belcher, P.D., Ihinger, P.D., Wang, L., Xu, Z., and Newman, S. (1997) New calibration of infrared measurement of water in rhyolitic glasses. Geochimica et Cosmochimica Acta, 61, 3089-300.

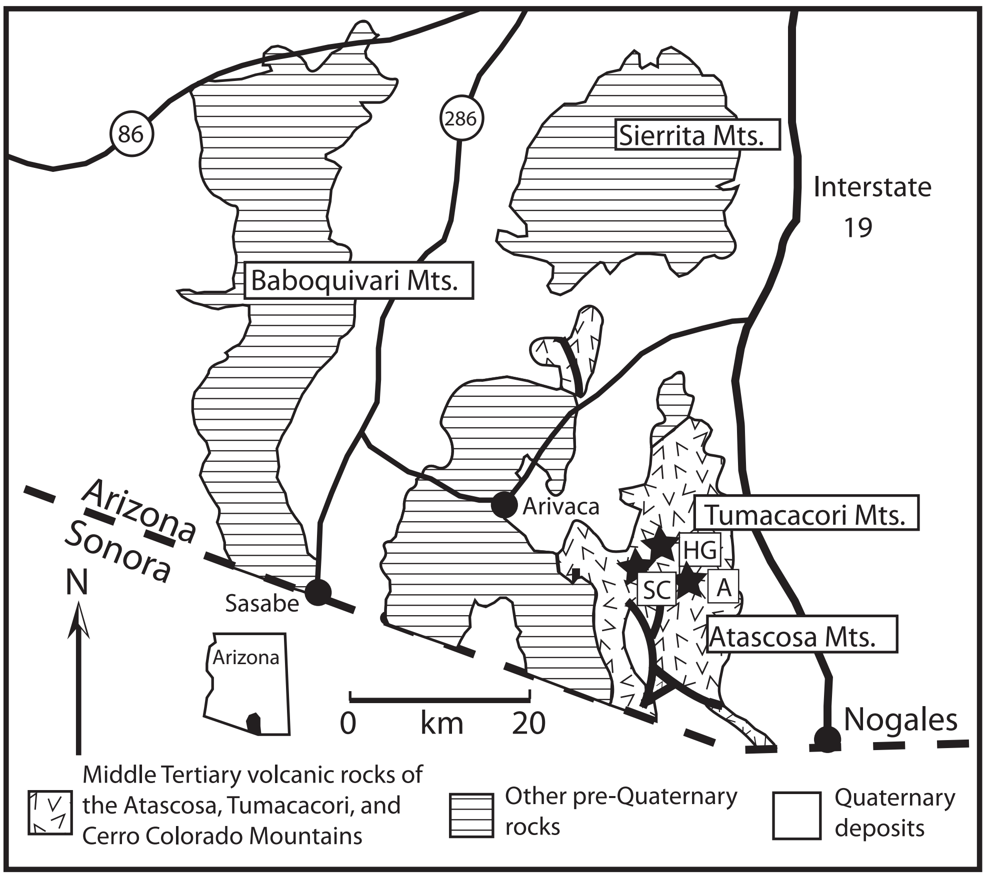

86
286
Sierrita Mts.
Interstate
19
Baboquivari Mts.
Arizona
Sonora
Arivaca
Tumacacori Mts.
HG
SC
A
N
Sasabe
Atascosa Mts.
Arizona
0
km
20
Nogales
Middle Tertiary volcanic rocks of the Atascosa, Tumacacori, and Cerro Colorado Mountains
Other pre-Quaternary rocks
Quaternary deposits

Fig. 1

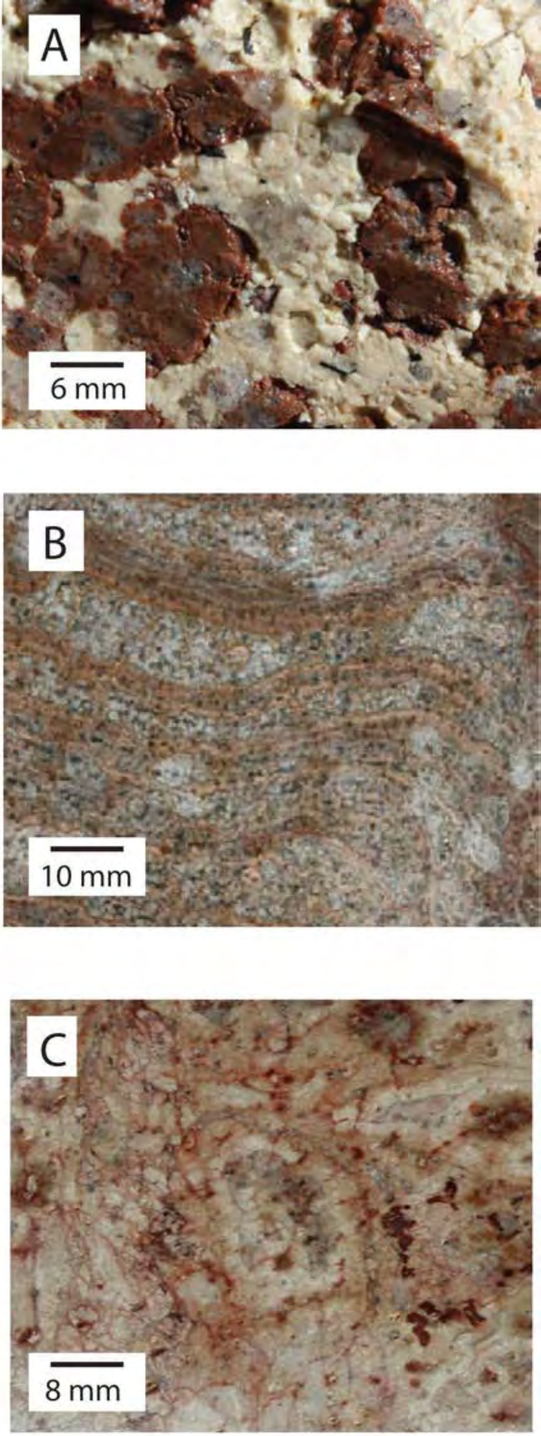

Figure 2.

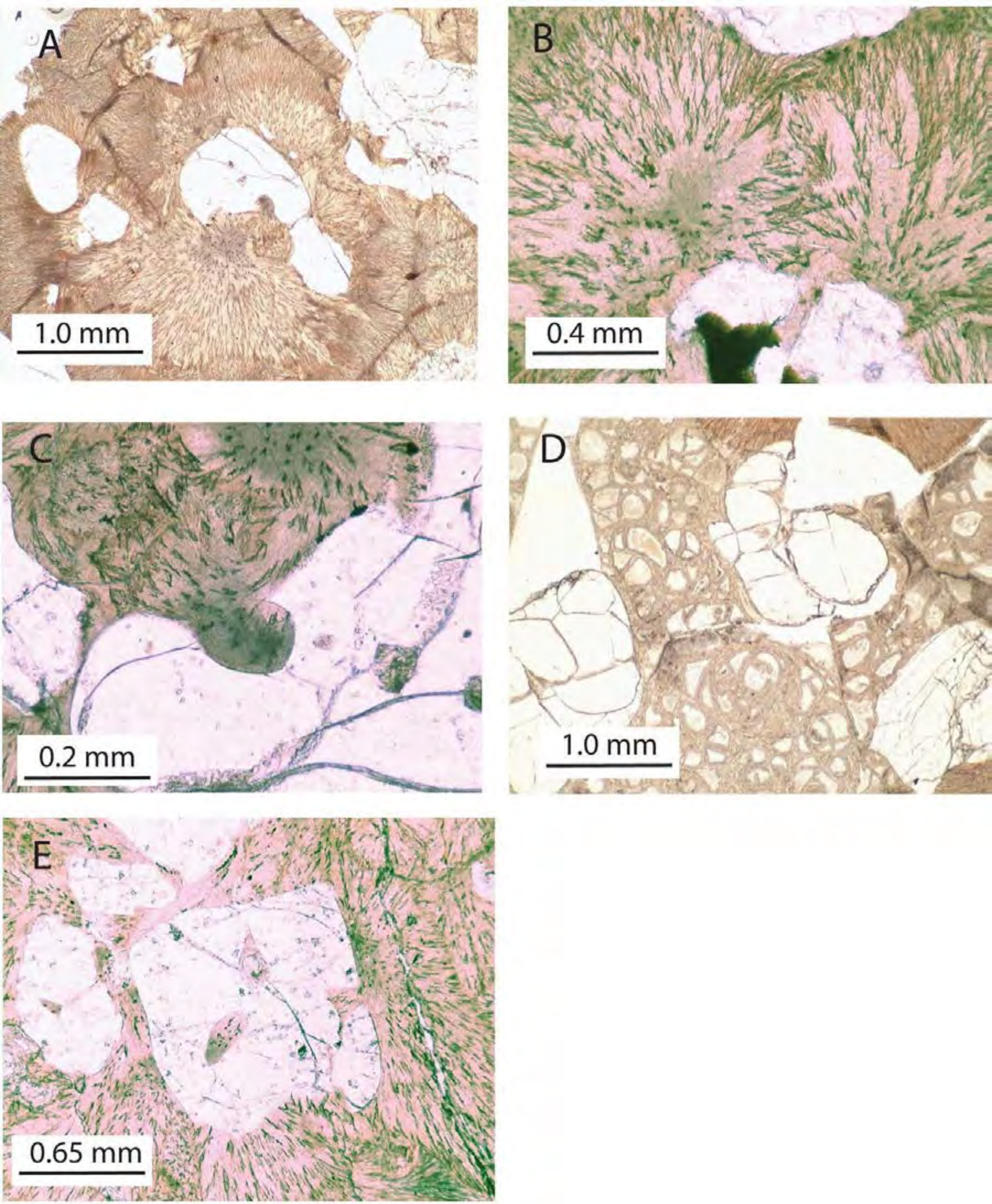

Figure 3.

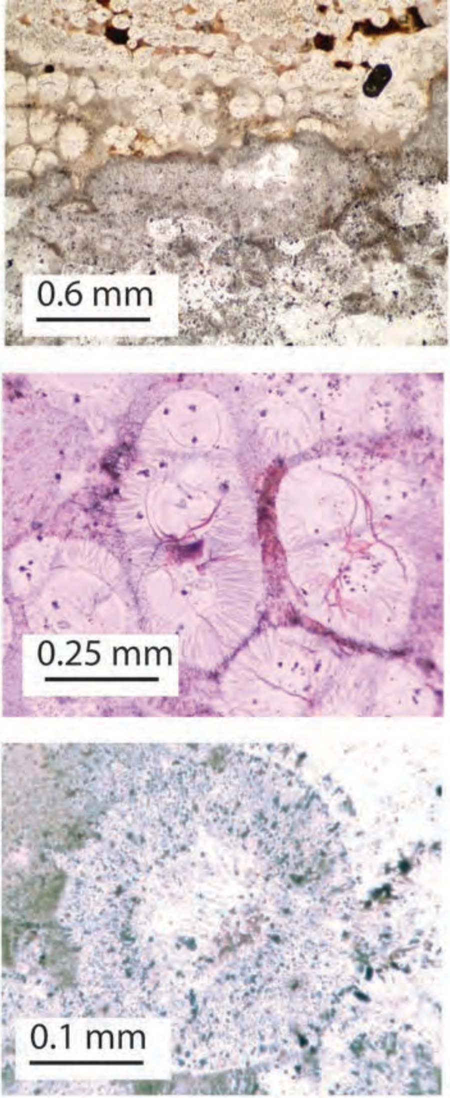

Figure 4.

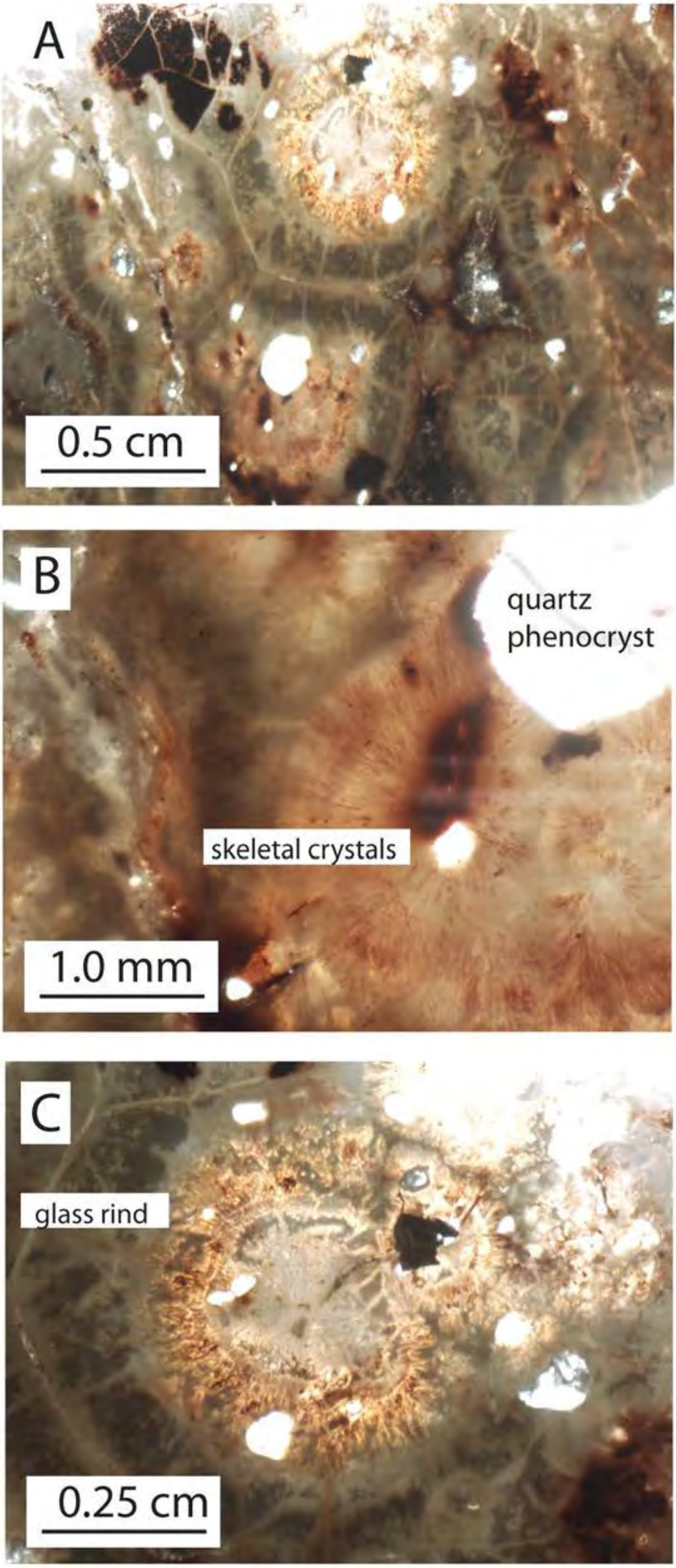
A
0.5 cm
B
quartz
phenocryst
skeletal crystals
1.0 mm
C
glass rind
0.25 cm

Figure 5

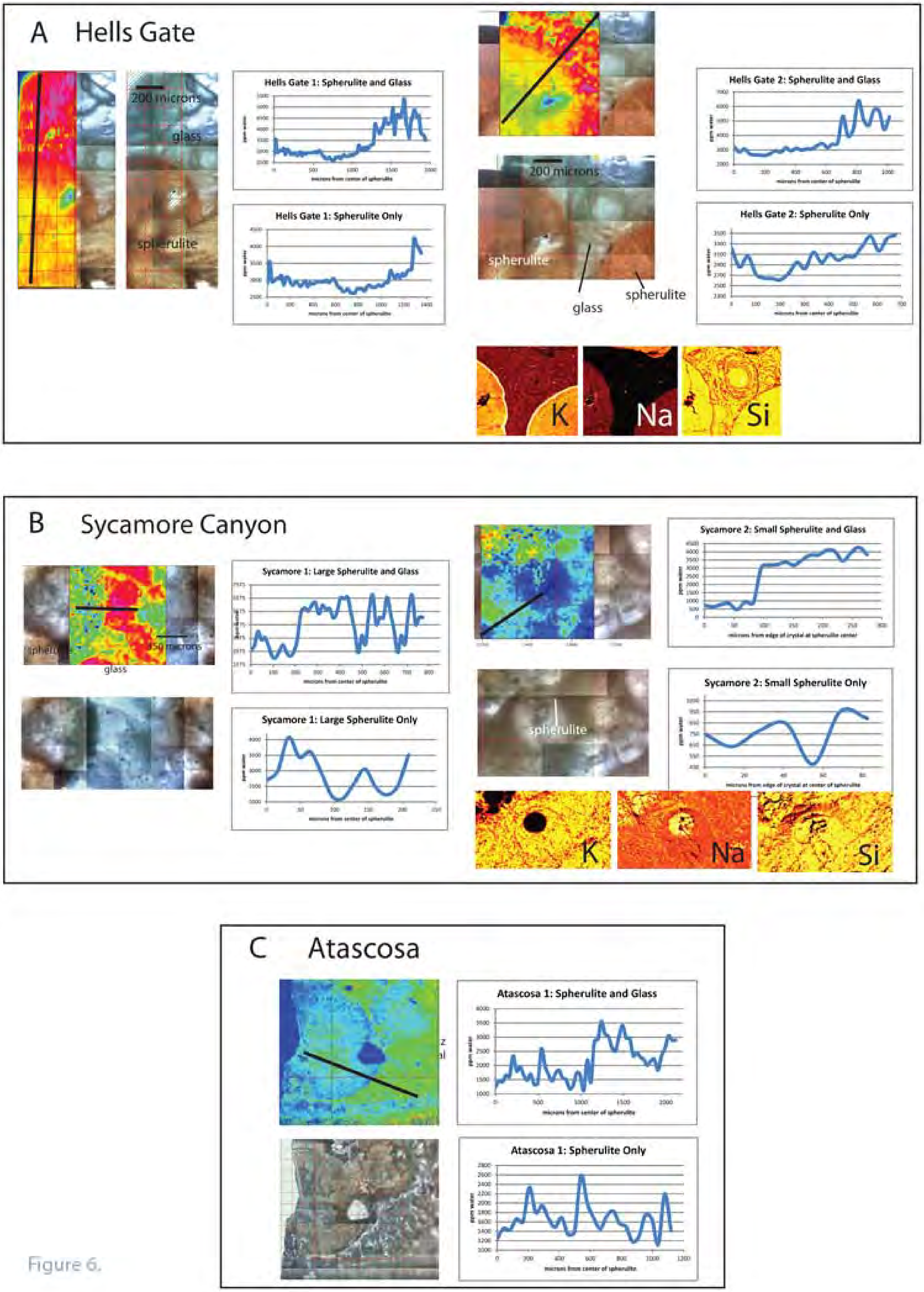
A Hells Gate
200 microns
glass
spherulite
Hells Gate 1: Spherulite and Glass
Hells Gate 1: Spherulite Only
200 microns
spherulite
glass
spherulite
Hells Gate 2: Spherulite and Glass
Hells Gate 2: Spherulite Only
K
Na
Si
B Sycamore Canyon
glass
Sycamore 1: Large Spherulite and Glass
Sycamore 1: Large Spherulite Only
Sycamore 2: Small Spherulite and Glass
spherulite
Sycamore 2: Small Spherulite Only
K
Na
Si
C Atascosa
Atascosa 1: Spherulite and Glass
Atascosa 1: Spherulite Only
microns from center of spherulite
ppm water

Figure 6.

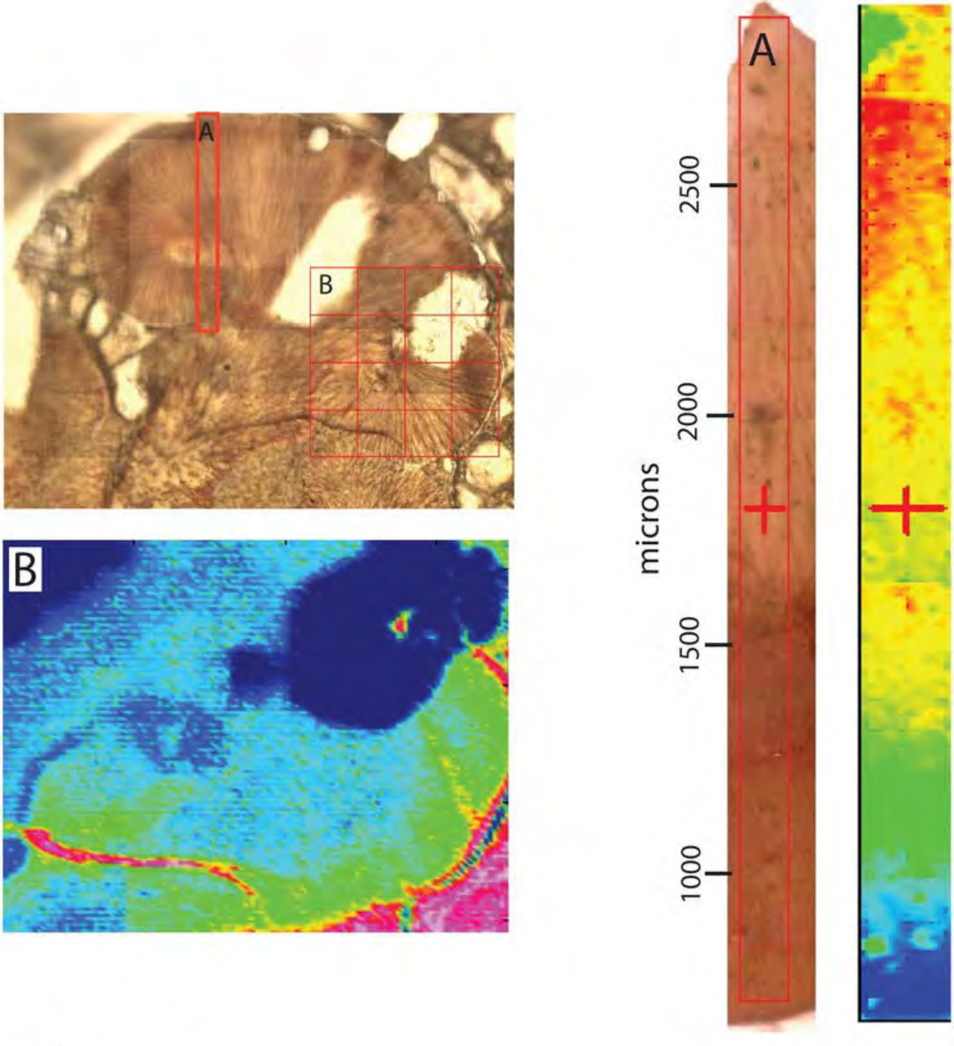

Figure 7.

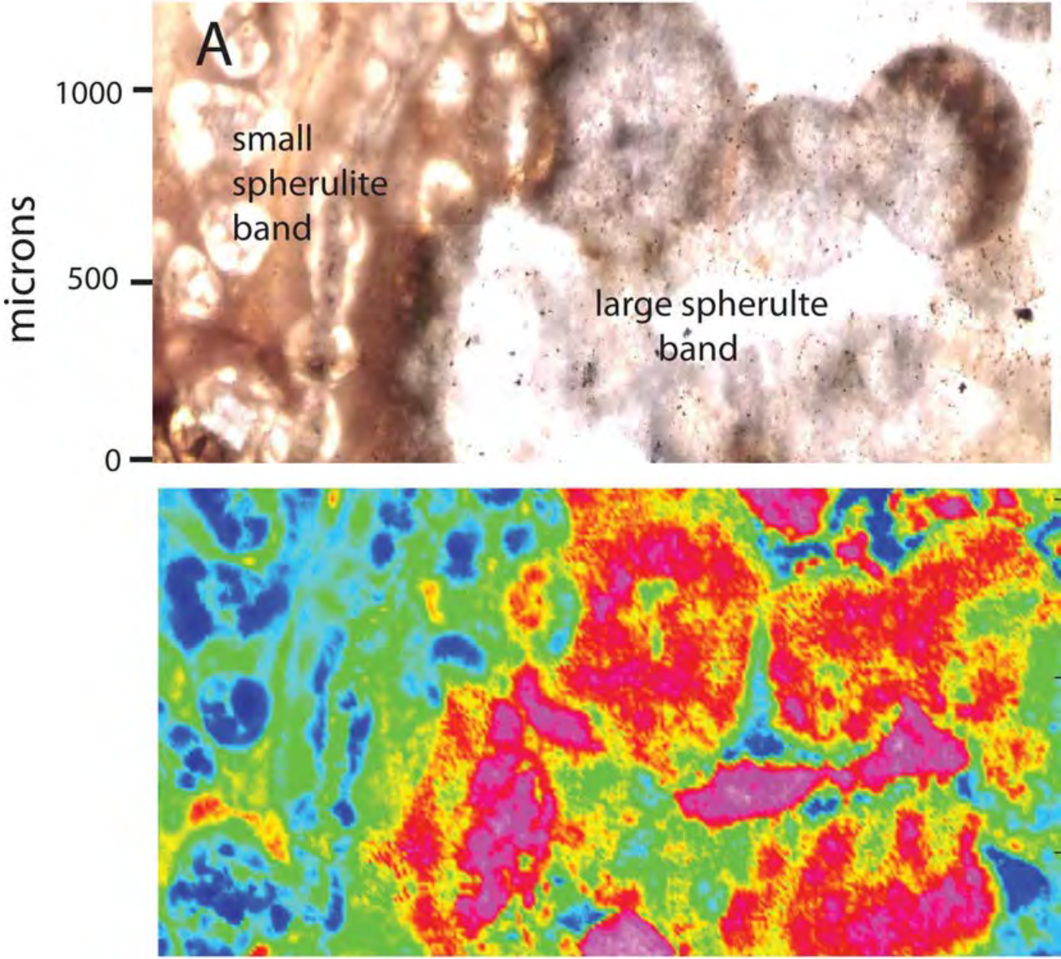
A
1000
500
0
microns
small
spherulite
band
large spherulte
band

Figure 8.

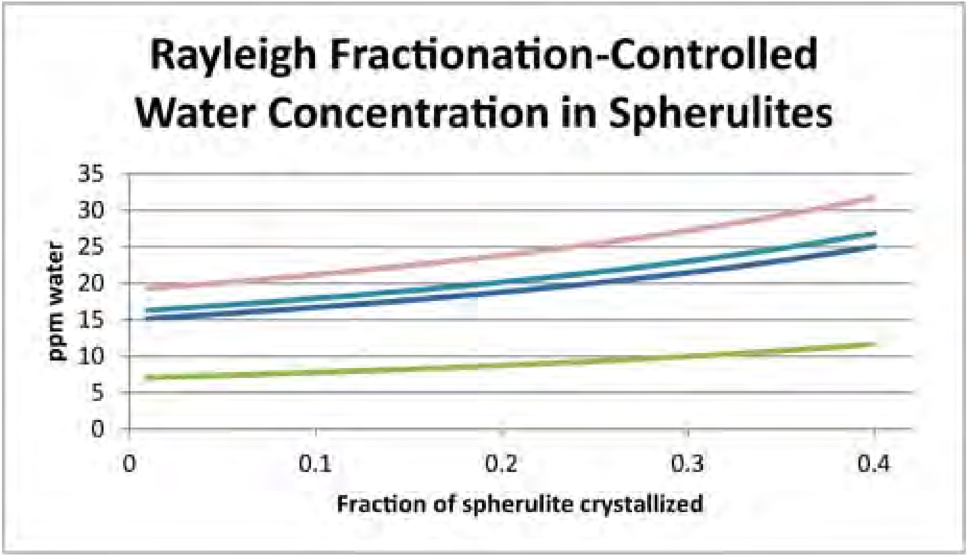
Rayleigh Fractionation-Controlled Water Concentration in Spherulites
35
30
25
20
15
10
5
0
ppm water
0
0.1
0.2
0.3
0.4
Fraction of spherulite crystallized

Figure 9

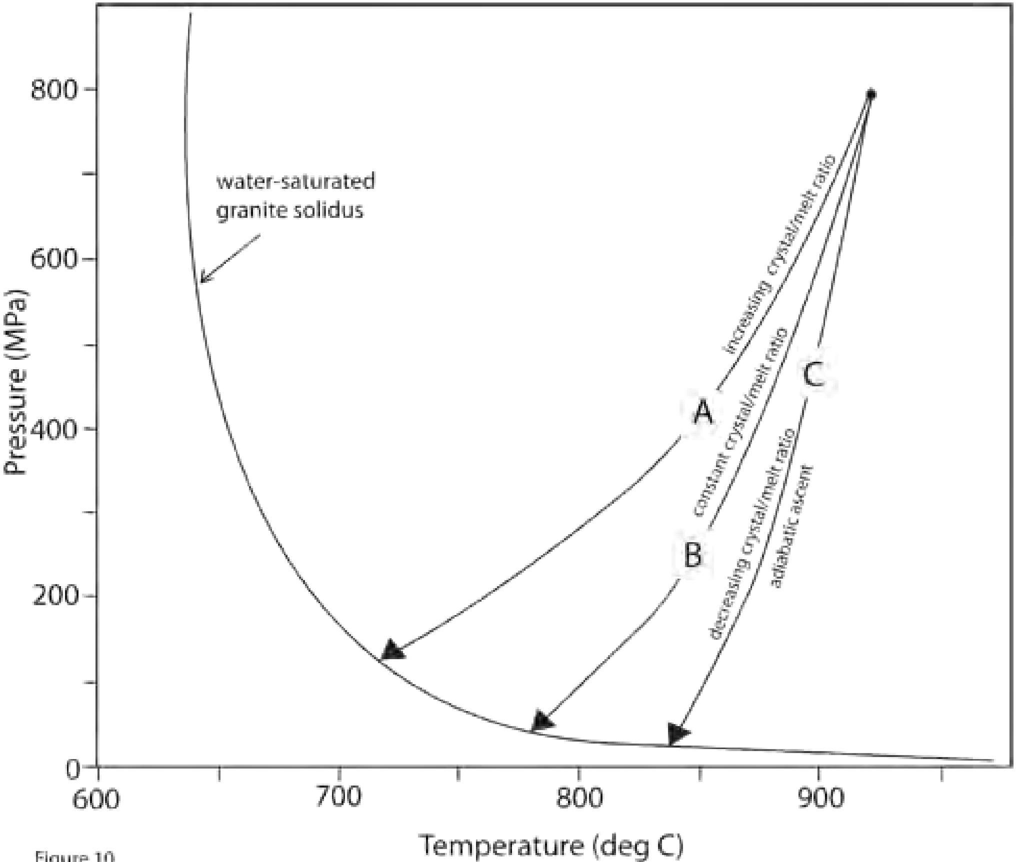

Pressure (MPa)
800
600
400
200
0
600
700
800
900
Temperature (deg C)
water-saturated
granite solidus
increasing crystal/melt ratio
constant crystal/melt ratio
decreasing crystal/melt ratio
adiabatic ascent
A
B
C

Figure 10.

Table 1. Major and Trace Element Analyses

	Sycamore Canyon	Hells Gate	Atascosa Lookout
Major element analyses in wt.%:			
SiO_2	76.39	76.55	77.89
TiO_2	0.10	0.13	0.07
Al_2O_3	12.79	13.26	12.64
MgO	0.03	1.01	0.59
FeO	0.49	0.07	0.03
CaO	0.34	0.35	0.03
MnO	0.03	1.37	0.11
Na_2O	3.99	2.10	2.88
K_2O	5.68	4.67	5.20
P_2O_5	0.03	0.04	0.02
Total	100.07	99.55	99.46
Trace element analyses in ppm:			
Nb	9	33	51
Zr	178	110	92

Y	14	26	32
Sr	803	338	6
U	0	8	13
Rb	84	162	365
Th	16	47	41
Pb	14	30	18
Ga	18	16	18
Zn	55	25	18
Ni	36	1	2
Cr	50	4	9
V	48	3	1
Ce	62	70	28
B	817	95	16

Table 2. Characteristics of the Three Rhyolitic Lava Flows

	Hells' Gate	Sycamore Canyon	Atascosa
Phenocrysts	abundant 0.5 to 3.0 mm diameter strongly resorbed quartz and alkali feldspar	sparse 0.1 to 0.5 mm diameter not resorbed quartz and alkali feldspar	sparse 0.25 to 1.0 mm diameter not resorbed quartz and alkali feldspar
Flow banded	no	yes	no
Spherulite size	1.2 to 3.0 mm diameter	light band spherulites: 0.4 to 0.6 mm diameter dark band spherulites: 0.1 to 0.2 mm diameter	0.4 mm to 1 cm diameter
crystal shape	blade-like	needle-like	needle-like
Water concentration trend in sanidine in spherulites	increases core to rim	increases core to rim	decreases slightly core to rim
Glass	unwelded perlite	mildly welded	strongly welded

Table 3. Water Concentrations Represented in Traverses Shown in Figure 6.

Hells Gate 1		Hells Gate 2		Sycamore 1		Sycamore 2		Atascosa	
microns from center of spherulite	ppm water*	microns from center of spherulite	ppm water*	microns from center of spherulite	ppm water*	microns from center of spherulite	ppm water*	microns from center of spherulite	ppm water*
0	2881	0	3221	0	2688	0	747	0	1249
21	3551	34	2860	16	2990	14	636	41	1457
42	2955	67	3062	32	4071	28	779	83	1429
62	2987	101	2722	48	3435	41	843	124	1665
83	3051	135	2647	64	3610	55	477	166	1609
104	3051	169	2636	80	2942	69	954	207	2331
125	3136	202	2615	97	2179	83	891	249	1803
146	2860	236	2743	113	2115	96**	3050	290	1942
167	3083	270	2945	129	2592	110	3177	332	1665
187	3051	303	2828	145	3053	124	3216	373	1484
208	2902	337	3136	161	2465	138	3374	415	1693
229	2860	371	2945	177	2226	151	3174	456	1332
250	2945	404	3104	193	2513	165	3502	498	1387
271	2892	438	2987	209	3515	179	3798	539	2580
291	2817	472	3062	225**	5491	193	3801	580	1998
312	2892	506	3062	241	5852	206	4088	622	1679
333	2977	539	3264	257	5600	220	4035	663	1457
354	2807	573	3444	273	6053	234	3433	705	1720
375	2924	607	3168	290	6255	248	3933	746	1831
396	2881	640	3402	306	5407	261	4270	788	1568
416	2902	674	3466	322	6037	275	3824	829	1498
437	2945	708**	5324	338	5743			871	1179
458	2945	741	3937	354	5793			912	1290
479	2945	775	4379	370	5105			954	1748
500	2945	809	6406	386	5457			995	1665
520	2998	843	5103	402	6591			1037	1124

541	2924
562	2998
583	3040
604	2924
625	2796
645	2764
666	2658
687	2679
708	2743
729	2626
749	2626
770	2615
791	2753
812	2732
833	2753
854	2668
874	2785
895	2849
916	2796
937	2785
958	2796
978	2860
999	2817
1020	2849
1041	2934
1062	2934
1082	3274
1103	3157
1124	3062
1145	3168
1166	3062
1187	3189
1207	3126
1228	3242

876	4694
910	5743
944	5688
977	4412
1011	5279

418	6515
434	6649
450	5407
466	4114
483	2477
499	3761
515	3106
531	5608
547	6809
563	4618
579	5121
595	5113
611	6649
627	5407
643	4114
659	2477
676	3761
692	3106
708	5608
724	6809
740	4618
756	5121
772	5113

1078	2192
1119	1415
1161**	2849
1202	2921
1244	3556
1285	3116
1327	3015
1368	2633
1410	2517
1451	3029
1493	3404
1534	2972
1575	2950
1617	2344
1658	2460
1700	2301
1741	2207
1783	2005
1824	2164
1866	2214
1907	1832
1949	2337
1990	2604
2032	3044
2073	2885
2114	2899

1249	3306
1270	3327
1291**	4230
1311	4064
1332	3943
1353	3805
1374	4042
1395	4147
1416	4501
1436	4318
1457	4230
1478	4302
1499	4418
1520	4954
1540	3772
1561	4567
1582	4666
1603	4523
1624	4595
1645	4948
1665	5351
1686	4285
1707	4059
1728	3612
1749	4330
1769	4550
1790	4871
1811	4749
1832	4517
1853	4617
1874	3877
1894	3777
1915	3728
1936	3518

* Water concentration in crystals is based on measurement of peak area in one orientation, with the resulting calculated water concentration multiplied by three because a molar absorption coefficient based on measurement in three mutually perpendicular orientations (Johnson and Rossman, 2003) was used. Water concentration in glass is based on measurement of peak height in one orientation and use of a molar absorption coefficient calculated on the basis of measurement in one orientation

** Denotes boundary between spherulite and glass

Molar absorption coefficients used in this work: sanidine crystals: 107000 L/mole H2O-cm^2 (Johnson and Rossman, 2003); glasses (Mandevillet et al., 2002; King et al., 2004): Hells Gate: 76.08 L/moleH2O-cm; Sycamore Canyon: 74.86 L/mole H2O-cm; Atascosa: 76.10 L/mole H2O-cm

Glass densities, calculated on the basis of composition (Fluegel, 2008): Hells Gate: 23306 g/L; Sycamore Canyon: 2329 g/L; Atascosa: 76.10 g/L

Thicknesses of samples: Hells Gate: 0.00184 cm; Sycamore Canyon: 0.00128 cm; Atascosa: 0.00123 cm

Table 4 Diffusion Coefficients and Water Diffusion Distance

	T in deg K	average wt% water	D m_2/sec	distance (micr in one year	ance (micr in one day	ance (microns) in one hour
Hells Gate	873	0.3758	9.48E-14	1728	91	18
	973	0.3758	2.97E-13	3059	160	33
	1073	0.3758	7.52E-13	4868	255	52
	1123	0.3758	3.11E-12	9902	519	106
Atascosa	873	0.4749	8.25E-14	1612	84	17
	973	0.4749	2.58E-13	2853	149	30
	1073	0.4749	6.54E-13	4539	238	49
	1123	0.4749	2.71E-12	9233	484	99
Sycamore Canyon						
light bands	873	0.4034	1.03E-13	1802	94	19
	973	0.4034	3.23E-13	3189	167	34
	1073	0.4034	8.18E-13	5075	266	54
	1123	0.4034	3.38E-12	10323	541	110
dark bands	873	0.1747	6.18E-14	1396	73	15
	973	0.1747	1.94E-13	2470	129	26
	1073	0.1747	4.91E-13	3931	206	42
	1123	0.1747	2.03E-12	7996	419	85